Aalborg Universitet

AALBORG UNIVERSITY

Single-cut Far-Field Antenna Radiation Pattern Reconstruction Accuracy Analysis in Compact Anechoic Chamber Setup

Jensen, Ole Kiel; Ji, Yilin; Zhang, Fengchun; Fan, Wei

Single-cut Far-Field Antenna Radiation Pattern Reconstruction Accuracy Analysis in Compact Anechoic Chamber Setup

Ole K. Jensen, Yilin Ji, Fengchun Zhang, and Wei Fan*

Department of Electronic Systems, Aalborg University, Aalborg, 9000, Denmark
okj@es.aau.dk, yilin@es.aau.dk, fz@es.aau.dk, *wfa@es.aau.dk

Abstract ─ In production testing, it is of importance to measure the key radiation parameters of an antenna under test (AUT), e.g., main beam peak and direction, sidelobes, and null depth and direction in a cost-effective setup with a short measurement time. As a result, practical measurement setups are often compact and equipped with only a few probes (or probe locations). However, these system limitations would introduce errors for antenna testing. This problem has become even more pronounced for 5G radios due to utilization of large-scale antenna configurations and high frequency bands. Spherical near-field measurements are nowadays an accurate and mature technique for characterizing AUTs, which however, necessitates a full spherical acquisition, leading to a long measurement time. Single-cut near-to-far-field transformation is a promising strategy since most of the key AUT parameters are available in the single-cut pattern and it requires much reduced measurement time. In this work, a simple and flexible scheme is proposed to evaluate errors introduced by limitations in practical setups for single-cut far-field (FF) antenna radiation pattern reconstruction, where the near-field data can be easily generated and modified according to the limitations introduced in practical multi-probe anechoic chamber setups, e.g., measurement distance, truncation range, and sampling interval. The reconstructed FF pattern is obtained using a commercial near-field to far-field transformation tool, SNIFT. The proposed scheme is numerically validated via comparing the reference FF pattern of a 4×8 uniform planar array composed of ideal Hertzian dipoles and reconstructed FF pattern. With the proposed scheme, the impact of practical system limitations on single-cut reconstruction accuracy can be easily analyzed.

Index Terms ─ Antenna pattern measurement, near-field far-field transformation, near field measurement, over-the-air testing, and single-cut antenna pattern.

I. INTRODUCTION

The ever-increasing demand for high data-rate, reliable and ubiquitous wireless communication has motivated research towards the fifth generation (5G) communication system and beyond [1-3]. This has been made possible, thanks to key radio frequency (RF) and antenna technologies, e.g., millimeter-wave and sub-THz frequency, large system bandwidth, large-scale antenna configuration, and integrated and low-cost RF front-end design. It is essential that we should measure large-scale antenna arrays (e.g., massive multiple-input multiple-output (MIMO) base stations) in a fast, accurate, and cost-effective manner. This has become more important and urgent due to the massive installation of large-scale antenna systems in cellular, satellite and military applications. The far-field antenna radiation pattern is one of the most important metrics to evaluate the radiated performance of the antenna system. However, it is getting more expensive and time-consuming, as the antenna under test (AUT) is getting larger and more complicated. Furthermore, over-the-air (OTA) testing is seen inevitable for future highly integrated antenna systems [4-9].

The antenna pattern measurement methods may be grouped into two categories including near-field (NF) and far-field (FF) ranges. Classical NF measurement techniques are based on the NF measurement of antennas, and the antenna FF is subsequently calculated through the near-field to far-field transformation. The amplitude and phase response of the AUT are sampled at a regular sampling grid with a well-designed measurement probe. Though highly accurate and mature in the industry, this method, however, requires both accurate amplitude and phase measurement of the AUT over a large sampling surface (i.e., full scan), and it also necessitates high-accuracy positioners [10]. The measurement time also becomes prohibitive when the electrical size of the AUT becomes large. Different FF methods have been extensively employed in the industry, e.g., direct-far-field (DFF), compact antenna test range (CATR) and plane wave generator (PWG) [11, 12]. The basic principle of DFF is that a plane wave at the antenna can be directly approximated if the measurement range is no smaller than the Fraunhofer FF distance. However, the requirement of measurement range might lead to large (and therefore expensive) anechoic chambers and link budget (i.e., small dynamic range) problems [13],

especially for large-scale AUTs. The CATR generates a plane wave using transformation with a parabolic reflector in a much shorter distance than the DFF method. The PWG can also enable over-the-air (OTA) testing directly in the far field at a reduced distance, by exciting the PWG array elements with suitably optimized complex coefficients. The CATR and PWG offer a good dynamic range due to reduced measurement range. However, the setup cost is rather expensive for massive deployment. In [14, 15], a mid-field (MF) method is proposed and validated to achieve OTA RF measurement, including AUT FF antenna patterns, transmit and receive performance metrics. The method presents some unique advantages. For example, it can significantly reduce the measurement distance; it only requires simple transformation from MF to FF results and it does not need phase measurement. However, it still requires some knowledge of the AUT (i.e., a grey-box solution) and measurement samples on two different radiated NF test distances to reconstruct the far-field results. A review of some recent advances in antenna measurements can be found in [16].

In practice, it is important and sometimes sufficient to rapidly determine several key antenna radiation parameters of the AUT, including antenna pattern peak power and direction, null depth and direction, and sidelobe level and direction, rather than to measure the full 3D radiation pattern. Single-cut FF patterns (e.g., in the E-plane or H-plane) are therefore of interest in practice since these key parameters are available in the single-cut pattern [17]. Furthermore, single-cut far field patterns can significantly reduce the NF measurement time. Much effort has been made to investigate the possibility of obtaining single-cut FF patterns from NF measurement data [17-21]. In this work, the objective is to investigate whether we can accurately reconstruct the single-cut FF pattern of the AUT in a cost-effective anechoic chamber setup equipped only with a few probe antennas. It is of importance to understand how limitations in practical setups would affect the reconstruction accuracy of the single-cut FF antenna array radiation pattern. More specifically, we are interested in how the single-cut FF pattern reconstruction accuracy is affected by practical systems:

- Compact measurement setup. A large measurement setup will take large floor-space, which can be very expensive, especially when many measurement facilities are required for massive production testing. For production testing purposes, the measurement range is often limited, e.g., up to 1 m.
- Short measurement time. Measurement time is one of the key performance indicators in

antenna measurement, due to the massive amount of AUTs to be tested and many RF parameters to be examined for a single AUT. In production testing, only a few measurement probe antennas might be available to reduce the measurement time. For single-cut measurements, this means that the measured accuracy might suffer from truncation error (introduced by a limited angular range covered by the probe antennas) and under-sampling error (introduced by the large sample spacing due to limited number of probe antennas).
- "Black-box" approach. In many cases, we might lack knowledge of the AUT design. Therefore, it is desirable that the testing method can be applied for any DUT, without knowledge of the DUT. This aspect is inherently covered by the spherical near field antenna measurement since the AUT is treated as black-box design.

The paper is organized as follows. We describe our strategy to reconstruct the single-cut FF antenna array pattern in Section II. After that, we numerically investigate how limitations in practical setups would affect the reconstruction accuracy of the single-cut FF antenna array radiation pattern. Section IV discusses the future work and concludes the paper.

II. METHOD

A. AUT configuration

Without loss of generality, a 4×8 UPA composed of ideal z-oriented Hertzian dipoles with an element spacing of 0.65λ at 3.5 GHz (i.e., 56 mm) is utilized as the AUT. The Hertzian dipole is selected for the array element since it is the simplest radiation source [22]. The array configuration is selected to mimic a realistic 5G base station antenna array configuration. The size of the UPA is $5.2\lambda \times 2.6\lambda$ at 3.5 GHz (i.e., 446 mm × 223 mm) including the antenna element size, and the array element excitations can be individually controlled for the AUT, to synthesize various antenna array radiation patterns. In the simulation, the mutual coupling among array elements is not considered for the sake of simplicity, though it is important for BS antenna performance [23]. To avoid a completely symmetric AUT radiation pattern (therefore potentially over-simplifying the research problem), 28 antenna elements (marked in grey) are excited with phase 0° while the rest 4 antenna elements (marked in black) are excited with phase $-90°$, as indicated in Fig. 1. Uniform amplitude excitations are allocated for all antenna elements in the AUT. Note that other array configurations and element excitations can be set as well following the same procedure.
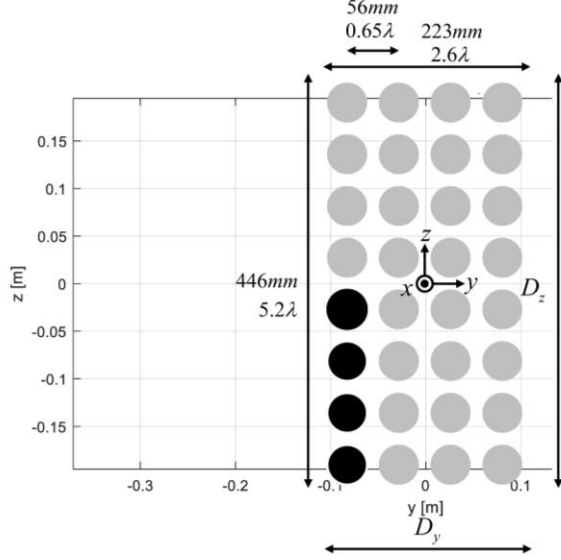
Fig. 1. An illustration of the AUT configuration and element excitations.

B. Problem statement

Following the standard spherical near field theory [24], the required number of spherical wave modes to fully reconstruct the AUT FF antenna pattern can be calculated according to the array geometry ($D_y = 2.6\lambda$, $D_z = 5.2\lambda$) as

$$N \approx \pi \frac{D_z}{\lambda} + \xi \approx 16 + \xi, \tag{1}$$

$$M \approx \pi \frac{D_y}{\lambda} + \xi \approx 8 + \xi, \tag{2}$$

where ξ is the margin [24, 25]. The maximum permissible sampling increments using standard spherical near field theory in θ and ϕ should satisfy, $\Delta_\theta < \frac{\pi}{N}$ and $\Delta_\phi < \frac{\pi}{M}$, respectively. Therefore, the number of spherical wave modes required is at minimum $M \cdot N = (8 + \xi)(16 + \xi) = 128 + 24\xi + \xi^2$. Using the standard spherical near field theory, we can obtain the full 3D FF pattern of the AUT, yet a large number of samples is required. As explained, for many applications, it is important to rapidly obtain the AUT FF pattern key parameters, including, e.g., array pattern peak power and direction, side-lobe power and direction, and null depth and direction, which are included the AUT single-cut FF antenna pattern within a certain angular region (e.g., ±50° around the main beam peak).

In this work, we aim to reconstruct the single-cut FF pattern in a cost-effective measurement setup, where the number of probe antennas is limited to around 10 and the measurement range is limited to 1 m. A diagram of the setup is shown in Fig. 2. Note that the maximum size for an AUT with far-field distance of 1m is $D = 207$ mm at 3.5 GHz. Therefore, the far-field criterion is not fulfilled for the considered AUT and measurement range. To reduce the setup cost and measurement time, it is of

importance to understand the impact of measurement range, number of probe antennas (i.e., finite samples) and truncation error (i.e., finite angular region covered by the probe antennas) on the accuracy of the reconstructed single-cut FF pattern. These aspects are considered in this work.
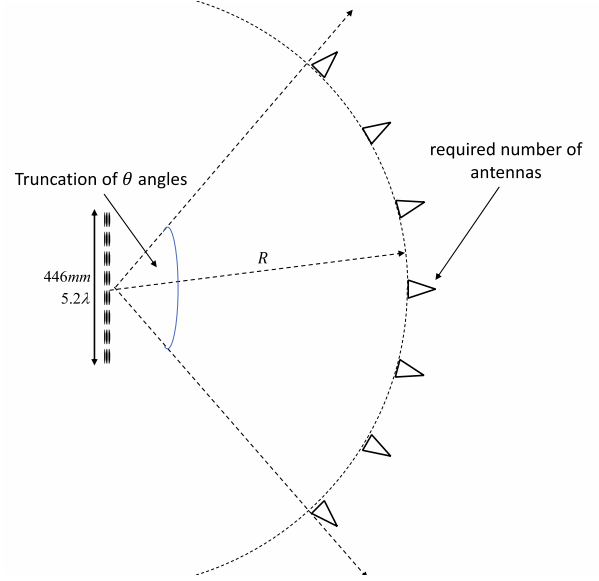

Fig. 2. Diagram of the multi-probe setup and a DUT.

In this article, two methods to obtain the AUT FF patterns are employed. With the first method, the NF and FF field pattern of the AUT composed of the 32 Hertzian dipoles with known excitation can be directly calculated according to the well-defined field radiation characteristics of Hertzian dipoles [22]. The other method to obtain the FF pattern is to use the spherical near-field to far-field transformation method. In our work, SNIFT developed by TICRA is utilized for this purpose [26]. The input NF data of SINFT is directly calculated from the known AUT (using the field pattern of the AUT), while the FF data is directly available at the SNIFT output. Ideal probe antennas (i.e., RF transparent probe antennas with isotropic antenna patterns) are assumed for the sake of simplicity, though it is not a limitation of SNIFT.

The calculated NF gain pattern at $R = 0.5$ m in Matlab is shown in Fig. 3, as an example. Using the NF data recorded at $R = 0.5$ m as input data, the FF pattern can be obtained using SNIFT, as shown in Fig. 3. The single-cut NF patterns (i.e., with $\phi = 0°$) at $R = 0.5$ m and FF distance are compared in Fig. 3. The FF pattern is not completely symmetric due to the non-symmetric AUT element excitation, as explained. The main beam and nulls in the NF pattern are not as obvious as in the FF pattern due to the small measurement distance, as expected. Therefore, there is a need for near-field to far-

field transformation techniques to reconstruct the FF results based on NF data.
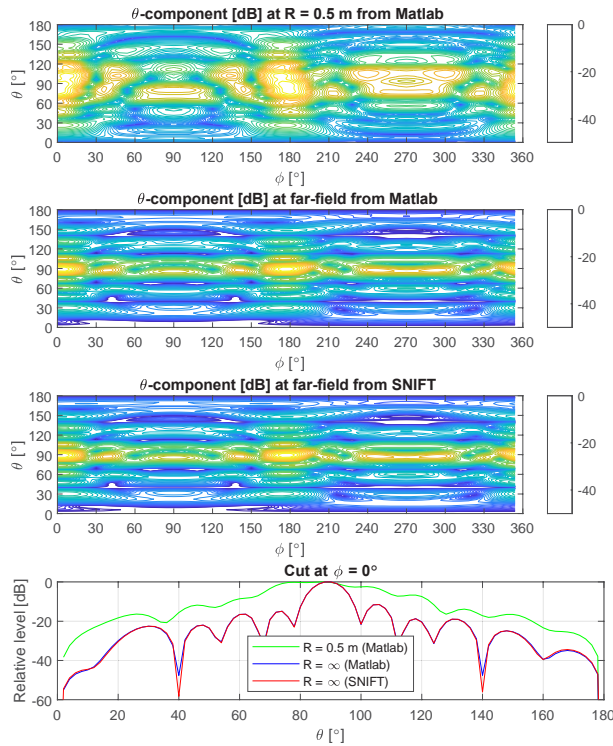

Fig. 3. Calculated NF pattern ($R = 0.5$ m) of the AUT in Matlab and FF pattern using SNIFT (input NF data at $R = 0.5$ m).

To validate whether our NF and FF calculations of the AUT based on radiated field of the Hertzian dipoles are correct, we can calculate the FF AUT pattern in Matlab and compare it with the FF pattern obtained from SNIFT, as shown in Fig. 3. The single-cut FF patterns using the two methods are also shown in Fig. 3. An excellent match is achieved within a range of 45 dB, which demonstrates the validity of our NF and FF calculations based on radiated field of the Hertzian dipoles.

C. Proposed strategy

To measure the ideal single-cut FF pattern, the measurement distance R should satisfy the far-field assumption while we have a sufficient number of samples, e.g., with 1° step to capture all details in the FF pattern. This, however, is not feasible for many measurement scenarios. As explained, it is desirable that we should reconstruct the single-cut FF pattern of the AUT in a fast and cost-effective manner. As for a practical multi-probe anechoic chamber setup, this implies a small measurement distance and a low number of probe antennas. In this work, we aim to reconstruct the single-cut FF pattern of the AUT based on single-cut

NF data in a practical setup. A framework to investigate the single-cut FF pattern reconstruction accuracy is proposed in this work, as illustrated in Fig. 4 and explained below.

1) The AUT is composed of ideal Hertzian dipoles, and therefore the AUT characteristics can be fully determined once the array configuration and array element excitations are set.

2) The reference FF pattern can be directly calculated in Matlab according to the field distribution of Hertzian dipoles.

3) The NF of the AUT at a distance R can also be directly calculated following the field distribution of in Hertzian dipoles in Matlab. The NF single-cut pattern (i.e., with $\phi = 0°$) can be modified according to the compact anechoic chamber configurations:

   a) Single-cut operation. To obtain the single-cut FF pattern of the AUT based on NF data, the following procedure is used. The NF pattern at $\phi = 0°$ is selected and copied to all other ϕ-values. Then the reconstructed NF data is used as the input data to obtain the FF pattern of the AUT using SNIFT. An example is shown in Fig. 5, where the NF AUT pattern at $R = 0.5$ m and the reconstructed NF data is shown. Then the reconstructed NF data is used as the input data to obtain the FF pattern of the AUT using SNIFT, as shown in Fig. 5. The reconstructed single-cut FF pattern (i.e., with $\phi = 0°$) is compared with the target calculated single-cut FF pattern in Fig. 5. A good match can be achieved, while small deviations in the sidelobes and null depths exist. This is introduced by the single-cut operation of the NF data with a small measurement range.

   b) Single-cut operation with truncation of θ range. The NF data can be truncated in θ, e.g., 30° to 150° to demonstrate the impact of truncation error introduced by a limited angle covered by the probe antennas. The NF data outside the truncation range is simply set to 0. Note that θ truncation is not seen at the output (FF) of SNIFT, while only the input data (NF) is truncated.

   c) Single-cut operation with increased sampling intervals. The sampling interval will have to be updated according to the number of available probe antennas in the measurement system. The NF data (input) is re-

sampled according to the sampling interval. The FF data (output) can be interpolated to make the pattern curve smoother.

4) The modified NF data at distance R can be obtained via copying the NF pattern at $\phi = 0°$ to all other ϕ-values.

5) We can then obtain the reconstructed FF pattern of the modified NF pattern from SNIFT.

6) In the end, we can extract the single-cut FF pattern from the reference and reconstructed results and compare.

With the proposed framework, we can flexibly modify the NF data introduced by limitations in practical systems, i.e., measurement distance R, truncation of θ range, and sampling intervals, and investigate the inaccuracies introduced by these limitations.
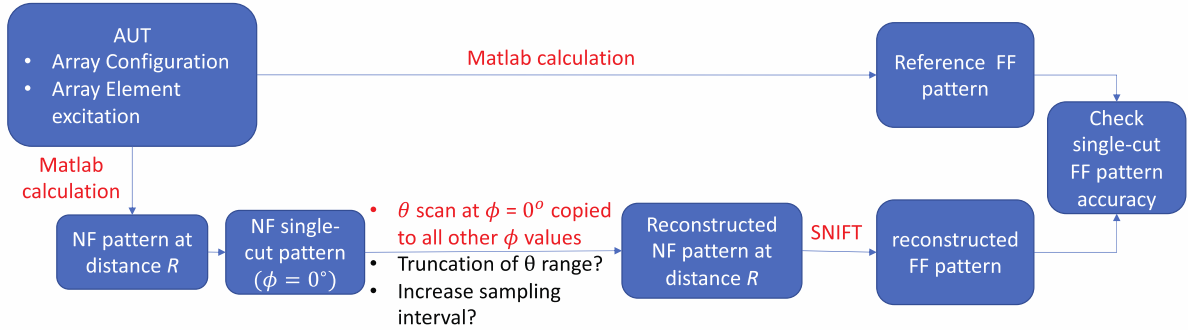

Fig. 4. The proposed simulation framework to investigate the single-cut FF pattern reconstruction accuracy.

III. SIMULATION RESULTS

A. Measurement distance R

The calculated FF pattern using Matlab and the FF pattern obtained from SNIFT (input data: calculated NF data at $R = 1$ m) are shown in Fig. 6. The two single-cut FF patterns (with $\phi = 0°$) are shown in Fig. 6 (bottom). As we can see, a better agreement is achieved, compared to the results in Fig. 5 (with NF data at $R = 0.5$ m). The improved accuracy is introduced by a larger measurement range, as expected. Generally speaking, a larger measurement distance would lead to less error in the single-cut FF pattern. It can be observed that the single-cut operation of the NF data will introduce negligible errors with $R = 1$ m for the considered AUT. Therefore, in the simulation below, $R = 1$ m is considered unless otherwise stated.

B. Truncation error

The next step is to investigate the impact of θ-range truncation on the single-cut FF pattern accuracy. For a practical system, we aim to determine the antenna pattern key parameters using the minimal required number of probe antennas. The key parameters, including main peak power and direction, first null depth and direction, and first side-lobe level and direction, are concentrated around $\theta = 90°$. Therefore, θ-range truncation might not affect the reconstruction accuracy of these key parameters. On the other hand, a large θ-range truncation with the same number of probe antennas (i.e., more concentrated probe configurations) also means a smaller sampling interval, which is beneficial to

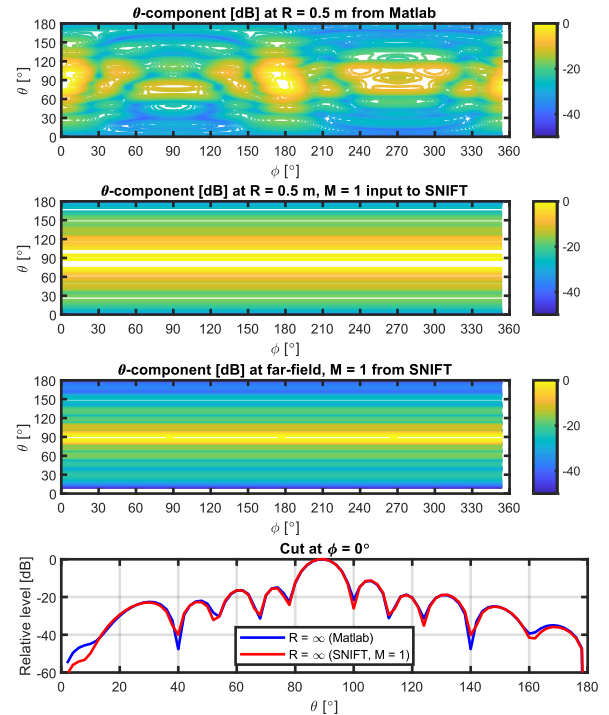the pattern reconstruction accuracy.

Fig. 5. Reconstructed FF AUT pattern in SNIFT (input NF data: modified AUT pattern at $R = 0.5$ m and pattern at $\phi = 0°$ is selected and copied to all other ϕ-values) (top) and comparison with target single-cut FF pattern (bottom).
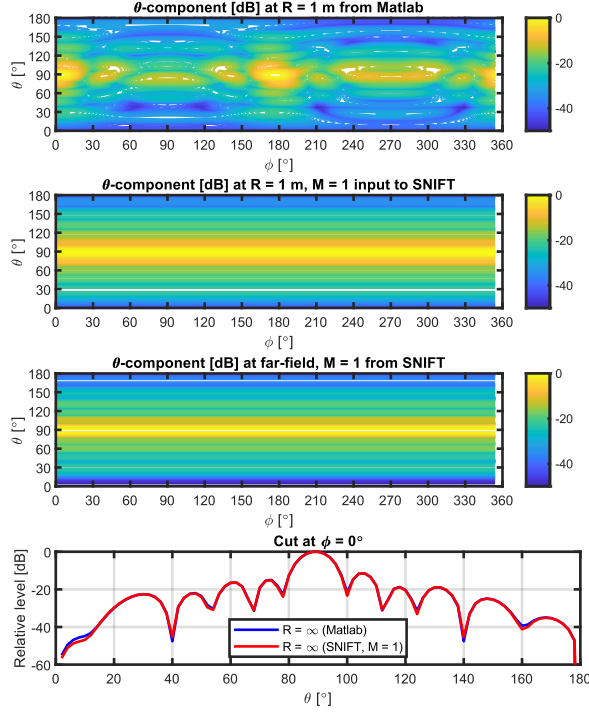
Fig. 6. Reconstructed FF AUT pattern in SNIFT (input NF data: modified AUT pattern at $R = 1$ m and pattern at $\phi = 0°$ is selected and copied to all other ϕ-values) (top) and comparison with target single-cut FF pattern (bottom).

The reconstructed single-cut FF patterns with θ truncation ranges $[0°, 180°]$ (i.e., no θ truncation), $[30°, 150°]$, $[45°, 135°]$, and $[60°, 120°]$ are shown and compared with the reference single-cut FF pattern in Fig. 7. As we can see, smaller θ-range truncations (i.e., θ truncation range $[30°, 150°]$ and $[45°, 135°]$) do not deteriorate the pattern reconstruction accuracy for the main lobe, the first null and the first side-lobe. However, a large all θ-range truncation (i.e., θ truncation range $[60°, 120°]$) leads to large deviations in the first null and also the side-lobe level as well. Therefore, the θ truncation range should be properly set in practical measurement systems to balance the measurement error and measurement time.

C. Number of probe antennas

The number of probe antennas is limited in practical measurement systems, due to cost and measurement time considerations. Therefore, it is important to understand the impact of the sampling interval on the single-cut FF radiation pattern reconstruction accuracy.

Following the standard spherical near field theory, the theoretical limit of the sampling interval is:

$$\Delta_\theta < \frac{180°}{\pi \frac{Dz}{\lambda} + \xi}. \qquad (3)$$

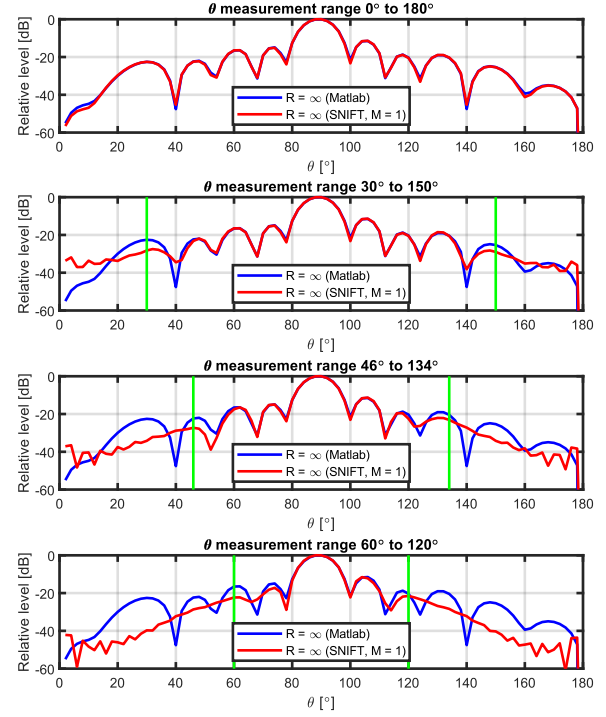That is, Δ_θ should be smaller than $12.6°$ without margin in principle to avoid errors introduced by under-sampling.

Fig. 7. Reconstructed single-cut FF patterns with θ truncation range $[0°, 180°]$, $[30°, 150°]$, $[45°, 135°]$ and $[60°, 120°]$.

The calculated FF pattern using Matlab (with sampling interval $\Delta_\theta = 5°$) is shown in Fig. 8. The FF pattern obtained from SNIFT using the modified NF data according to measurement setup (θ-scan at $\phi = 0°$, $\Delta_\theta = 5°$, θ truncation to $[30°, 150°]$, and measurement distance $R = 1$ m) is shown in Fig. 8. The single-cut FF patterns are compared in Fig. 8, where a good agreement can be observed. This is expected, since the sampling interval satisfies the theoretical limit. The truncation operation introduces some deviation for the angular region outside of the truncation region, as explained. This measurement system configuration would result in around 25 probe positions.

To be consistent with the simulation results shown so far (i.e., with $\Delta_\theta = 1°$), the output FF pattern from SNIFT (i.e., with $\Delta_\theta = 5°$) can also be interpolated, as shown in Fig. 8. Note that interpolation can be used to smooth the curve, while the reconstruction accuracy cannot be improved.
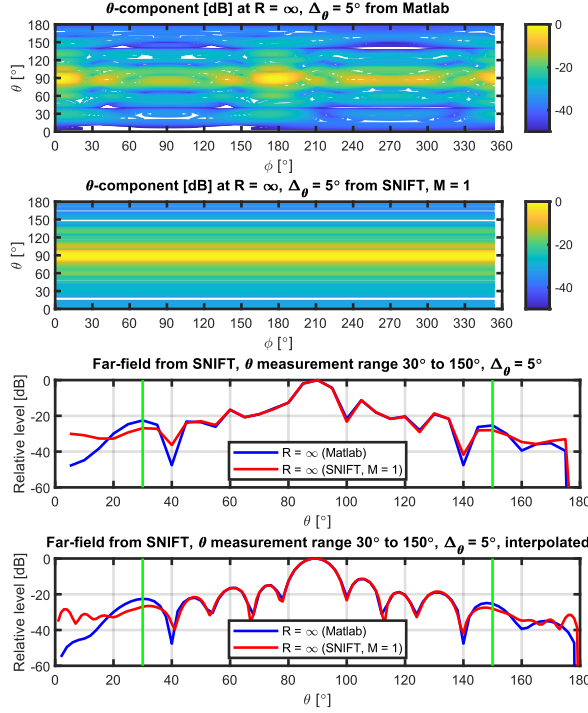
Fig. 8. The reference single-cut FF pattern and the interpolated reconstructed single-cut FF pattern with $\Delta_\theta = 5°$.
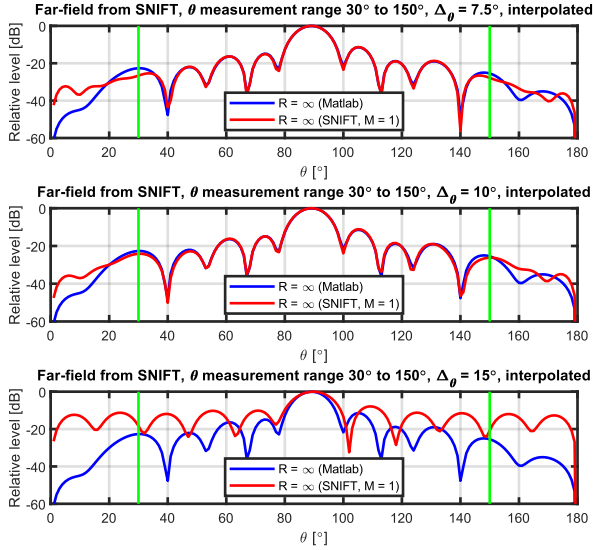

Fig. 9. Reconstructed FF single-cut pattern with sampling intervals $\Delta_\theta = 7.5°$, $\Delta_\theta = 10°$, and $\Delta_\theta = 15°$, respectively.

In Fig. 9, the θ truncation range is kept at $[30°, 150°]$ and interpolation is applied. Sampling intervals $\Delta_\theta = 7.5°$, $\Delta_\theta = 10°$, and $\Delta_\theta = 15°$ are set, respectively. As we can observe, if the theoretical limit is satisfied (i.e., $\Delta_\theta < 12.6°$), no errors will be introduced due to sampling. However, if the theoretical limit is violated (e.g., $\Delta_\theta = 15°$), large deviations in the main lobe, side-lobes and nulls can be observed. Therefore, for single-cut FF antenna pattern reconstruction, it is important that the sampling criteria satisfies the theoretical limit.

IV. CONCLUSION AND FUTURE WORK

In this work, the focus is on how limitations introduced in practical antenna measurement setups, e.g., measurement range, truncation error, sampling intervals would affect the single-cut far-field pattern reconstruction accuracy of the AUT. To address this problem, a simple and flexible scheme is proposed, where the near-field data can be generated and modified according to practical setup constraints. In this way, we can easily check how the reconstruction accuracy is affected by different settings. A 4×8 UPA composed of z-oriented ideal Hertzian dipoles with element spacing 0.65λ at 3.5 GHz (i.e., 56 mm) is utilized as the AUT. Extensive numerical simulations have been performed to demonstrate the impact of measurement range, truncation error and sampling interval on the reconstruction accuracy. We have shown in numerical simulations that we can accurately reconstruct the single-cut far-field pattern of the considered AUT with $R = 1$ m, a truncation range of $[30°, 150°]$, and a sampling interval of $10°$.

There is some logic extension of the current work. The numerical simulations in the work are based on a UPA with ideal z-oriented Hertzian dipoles. It is of interest to investigate how well the proposed scheme works with more realistic antenna arrays (e.g., CST simulated or real array). The analysis is based on one specific case of AUT element excitations as explained in the AUT configuration section. We can also repeat the procedure to check more AUT excitations, to see whether the considered scenario is typical. For truncation error analysis, the data outside the truncation range is directly set to 0. We can also investigate whether we can improve the reconstruction accuracy by applying a window-function with the truncation. Furthermore, probe pattern correction should be considered for real measurements, which is not considered in our current work. It is also logic to investigate how the well proposed scheme works for planar scanning measurements.

REFERENCES

[1] C. Huang, R. Wang, P. Tang, R. He, B. Ai, Z. Zhong, C. Oestges, and A. F. Molisch, "Geometry-

cluster-based stochastic MIMO model for vehicle-to-vehicle communications in street canyon scenarios," *IEEE Transactions on Wireless Communications*, vol. 20, no. 2, pp. 755-770, 2021.

[2] K. Guan, B. Peng, D. He, J. M. Eckhardt, S. Rey, B. Ai, Z. Zhong, and T. Kürner, "Channel characterization for intra-wagon communication at 60 and 300 GHz bands," *IEEE Transactions on Vehicular Technology*, vol. 68, no. 6, pp. 5193-5207, 2019.

[3] B. Peng, K. Guan, A. Kuter, S. Rey, M. Patzold, and T. Kuerner, "Channel modeling and system concepts for future terahertz communications: Getting ready for advances beyond 5G," *IEEE Vehicular Technology Magazine*, vol. 15, no. 2, pp. 136-143, 2020.

[4] W. Fan, P. Kyosti, M. Rumney, X. Chen, and G. F. Pedersen, "Over-the-air radiated testing of millimeter-wave beam-steerable devices in a cost-effective measurement setup," *IEEE Communications Magazine*, vol. 56, no. 7, pp. 64-71, 2018.

[5] X. Chen, M. Zhang, S. Zhu, and A. Zhang, "Empirical study of angular–temporal spectra in a reverberation chamber," *IEEE Transactions on Antennas and Propagation*, vol. 66, no. 11, pp. 6452-6456, 2018.

[6] W. Xue, F. Li, and X. Chen, "Effects of signal bandwidth on total isotropic sensitivity measurements in reverberation chamber," *IEEE Transactions on Instrumentation and Measurement*, vol. 70, pp. 1-8, 2021.

[7] X. Chen, W. Fan, L. Hentilä, P. Kyösti, and G. F. Pedersen, "Throughput modeling and validations for MIMO-OTA testing with arbitrary multipath," *IEEE Antennas and Wireless Propagation Letters*, vol. 17, no. 4, pp. 637-640, 2018.

[8] P. Kyösti, W. Fan, and J. Kyröläinen, "Assessing measurement distances for OTA testing of massive MIMO base station at 28 GHz," in *2017 11th European Conference on Antennas and Propagation (EUCAP)*, pp. 3679-3683, 2017.

[9] Y. Ji, W. Fan, G. F. Pedersen, and X. Wu, "On channel emulation methods in multiprobe anechoic chamber setups for over-the-air testing," *IEEE Transactions on Vehicular Technology*, vol. 67, no. 8, pp. 6740-6751, 2018.

[10] F. D'Agostino, F. Ferrara, C. Gennarelli, R. Guerriero, and M. Migliozzi, "Probe position errors corrected near-field-far-field transformation with spherical scanning," *Applied Computational Electromagnetics Society Journal*, vol. 31, no. 2, 2016.

[11] Z. Qiao, Z. Wang, W. Fan, X. Zhang, S. Gao, and J. Miao, "Low scattering plane wave generator design using a novel non-coplanar structure for near-field over-the-air testing," *IEEE Access*, vol.

[12] Y. Zhang, Z. Wang, X. Sun, Z. Qiao, W. Fan, and J. Miao, "Design and implementation of a wideband dual-polarized plane wave generator with tapered feeding nonuniform array," *IEEE Antennas and Wireless Propagation Letters*, vol. 19, no. 11, pp. 1988-1992, 2020.

[13] X. Chen, "Measurement uncertainty of antenna efficiency in a reverberation chamber," *IEEE Transactions on Electromagnetic Compatibility*, vol. 55, no. 6, pp. 1331-1334, 2013.

[14] H. Kong, Z. Wen, Y. Jing, and M. Yau, "Midfield over-the-air test: A new OTA RF performance test method for 5G massive MIMO devices," *IEEE Transactions on Microwave Theory and Techniques*, vol. 67, no. 7, pp. 2873-2883, 2019.

[15] H. Kong, Y. Jing, Z. Wen, and L. Cao, "Mid-field OTA RF test method: new developments and performance comparison with the compact antenna test range (CATR)," in *2020 14th European Conference on Antennas and Propagation (EuCAP)*, pp. 1-5, 2020.

[16] M. Sierra-Castañer, "Review of recent advances and future challenges in antenna measurement," *Applied Computational Electromagnetics Society Journal*, vol. 33, no. 1, 2018.

[17] R. Cornelius, T. Salmerón-Ruiz, F. Saccardi, L. Foged, D. Heberling, and M. Sierra-Castañer, "A comparison of different methods for fast single-cut near-to-far-field transformation [euraap corner]," *IEEE Antennas and Propagation Magazine*, vol. 56, no. 2, pp. 252-261, 2014.

[18] S. Omi, T. Uno, and T. Arima, "Single-cut near-field far-field transformation technique employing two-dimensional plane-wave expansion," *IEEE Antennas and Wireless Propagation Letters*, vol. 17, no. 8, pp. 1538-1541, 2018.

[19] X. Li, G. Wei, L. Yang, and B. Liao, "Fast determination of single-cut far-field pattern of base station antenna at a quasi-far-field distance," *IEEE Transactions on Antennas and Propagation*, vol. 68, no. 5, pp. 3989-3996, 2020.

[20] Y. Sugimoto, H. Arai, T. Maruyama, M. Nasuno, M. Hirose, and S. Kurokawa, "Fast far-field estimation method by compact single-cut near-field measurements for electrically long antenna array," *IEEE Transactions on Antennas and Propagation*, vol. 66, no. 11, pp. 5859-5868, 2018.

[21] F. Rodríguez Varela, B. G. Iragüen, and M. Sierra-Castañer, "Undersampled spherical near-field antenna measurements with error estimation," *IEEE Transactions on Antennas and Propagation*, vol. 68, no. 8, pp. 6364-6371, 2020.

[22] C. A. Balanis, *Modern Antenna Handbook*. John Wiley & Sons, 2011.

[23] X. Chen, S. Zhang, and Q. Li, "A review of mutual

coupling in MIMO systems," *IEEE Access*, vol. 6, pp. 24 706-24 719, 2018.

[24] J. E. Hansen, "Spherical near-field antenna measurements," *Peter Peregrinus Ltd. (IEE Electromagnetic Waves Series 26), IET*, vol. 26, 1988.

[25] F. Jensen and A. Frandsen, "On the number of

modes in spherical wave expansions," *Proc. 26th AMTA*, vol. 2, no. 1, pp. 489-494, 2004.

[26] F. Jensen, "SNIFT-computer program for spherical near-field far-field technique, volume 2," *NASA STI/Recon Technical Report N*, vol. 77, p. 23328, 1976.